Detecting the mitigation of fused silica roughening after Ion Beam Figuring

Issued by ***J. Hołyszko*** (INAF/OAB), ***B. Salmaso*** (INAF/OAB), ***M. Ghigo*** (INAF/OAB),

IBF by ***M. Ghigo*** (INAF/OAB)

MFT measurements by ***J. Hołyszko*** (INAF/OAB) and ***B. Salmaso*** (INAF/OAB)

CCI measurements by ***L. Arcangeli*** (MLT)

SEM measurements by ***F. Passaretti*** (ICMATE-CNR-Lecco)

Reviewed by ***D. Spiga*** (INAF/OAB)

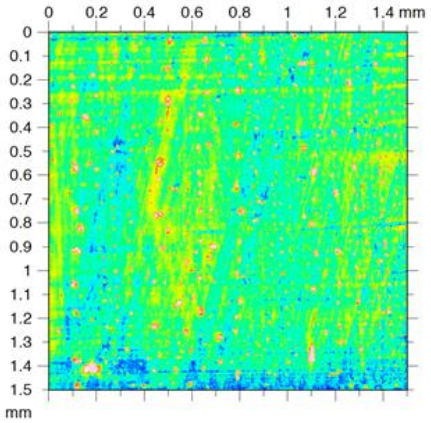

CCI image of a portion of a Wolter I Fused Silica segment, processed with IBF at 36 mm distance from the ion source

Istituto Nazionale di Astrofisica (INAF)

Via del Parco Mellini, 00100 Roma, Italy

Osservatorio Astronomico di Brera (OAB)

Via Brera 28, 20121 Milano, Italy

Via E. Bianchi 46, 23807 Merate, Italy

Contents

Reference Documents

[RD1]. Pareschi, G., Basso, S., Civitani, M., Ghigo, M., Parodi, G., Pelliciari, C., Salmaso, B., Spiga, D., Vecchi, G., *Beyond Chandra (towards the X-ray Surveyor mission): possible solutions for the implementation of very high angular resolution X-ray telescopes in the new millennium based on fused silica segments,* **Proceedings of SPIE** 9905, 99051T (2016)

[RD2]. A. Schindler, T. Haensel, D. Flamm, W. Frank, G. Boehm, F. Frost, R. Fechner, F. Bigl, B. Rauschenbach, *Ion Beam and Plasma Jet Etching for Optical Component Fabrication,* Lithographic and Micromachining Techniques for Optical Component Fabrication, **Proceedings of SPIE** Vol. 4440, 217-277 (2001)

[RD3]. Wilson, S.R., Reicher, D.W., Kranenberg, C.F., McNeil, J.R., White, P.L., *Ion beam milling of fised silica for window fabrication*, **Proceedings of SPIE** 1441 (1990)

[RD4]. Thienot, E., Domingo, F., Cambril, E., Gosse, C., *Reactive ion etching of glass for biochip application: composition effects and surface damage*, **Microelectronic Engineering**, Vol. 83, 1155-1158 (2006)

[RD5]. Zeze, D.A, Forrest, R.D., Carey, J.D., Cox, D.C., Robertson, I.D., Weiss, B.L., Silva, S.R.P., *Reactive Ion Etching of quartz and Pyrex for microelectronic application*, **Journal of Applied Physics**, Vol. 92, No. 7 (2002)

[RD6]. W. Liao, Y. Dai, X. Xie, L. Zhou, *Morphology evolution of fused silica surface during ion beam figuring of high-slope optical components,* **Applied Optics**, Vol. 52, 3719-3725 (2013)

Acronyms

CCI	Coherence Correlation Interferometry
CNR	Consiglio Nazionale delle Ricerche
CTE	Coefficient of Thermal Expansion
FIF	Five-axis Ion beam Figuring
IBF	Ion Beam Figuring
ICMATE	Istituto di Chimica della Materia Condensata e di Tecnologie per l'Energia
INAF	Istituto Nazionale di Astrofisica
IRP	Intelligent Robotic Polisher
MFT	MicroFinish Topographer
ML	Media Lario
OAB	Osservatorio Astronomico di Brera
PSD	Power Spectral Density
PV	Peak to Valley
RMS	Root Mean Square
RIE	Reactive Ion Etching
SEM	Scanning Electron Microscope
TIF	Three-axis Ion beam Figuring

1 Introduction

In order to look beyond Chandra, the Lynx/XRS mission has been proposed in USA and is currently studied by NASA. The optic will have an effective area of 2.5 m^2 and an angular resolution of 0.5 arcsec HEW at 1 keV. In order to fulfil these requirements, different technologies are considered, with the approaches of both full and segmented shells (that, possibly, can be also combined together). Concerning the production of segmented mirrors, a variety of thin substrates (glass, metal, silicon) are envisaged, to be possibly produced using both direct polishing or replication methods. We are developing a technology based on fused silica (SiO_2) segmented substrates [RD1], owing to the low CTE of Fused Silica and its high chemical stability, compared to other glasses. Thin SiO_2 segmented substrates (typically 2 mm thick) are figured in three steps with the equipment present in OAB laboratories: the first step is done by bonnet polishing on the 1200 model of the IRP (Intelligent Robotic Polisher) series machine made by Zeeko Ltd. in UK; the spatial frequencies error not correctable by bonnet polishing can be smoothed out in a second step by equipping the robotic arm with tailored pitch tools; the third and last step is accomplished by the Ion Beam Figuring (IBF) process, to remove the remaining few hundred of nanometers in the low frequency range. In this process, it is very important the IBF to preserve the quality of the surface roughness. Preliminary tests with IBF, carried out on a Fused Silica Wolter I segment, cut from a closed shell, produced a very promising result in terms of figure [RD1]. Anyway, some issue on the surface roughness of the segment after IBF was observed.

We have therefore searched throughout the literature, aiming at understanding the roughness degradation of Fused Silica with IBF, and made some IBF experiments on flat fused silica wafers with a thickness of 1 mm and a diameter of 100 mm, working at different distance from the ion source, in order to mitigate the problem.

2 Roughness degradation on Wolter I Fused Silica segment

Several segments were cut from a closed Fused Silica shell [RD1]. In particular, one (Fig. 1) was selected for its lower content in mid-frequency errors (spatial wavelengths around 7-8 mm), and it was processed with the IBF to remove the low-frequency deviation from the Wolter I profile.

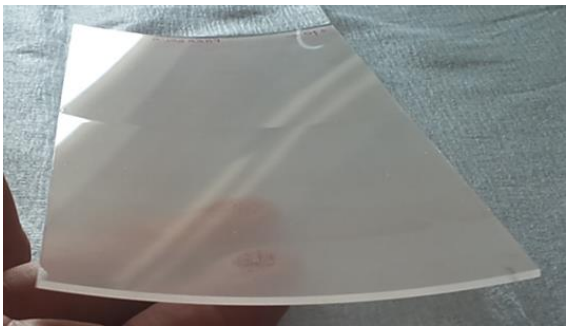

Fig. 1: Wolter I segment cut out a closed shell of Fused Silica (100 mm × 200 mm × 2 mm).

The IBF process was performed positioning the sample at 36 mm from the ion source, and with the 15 mm grids. Despite the good result in terms of profile correction, a roughness degradation was observed (Figs. 2-3-4). It was measured with the Nomarsky microscope and the MicroFinish Topographer (MFT) operated at OAB, and the CCI operated at ML.

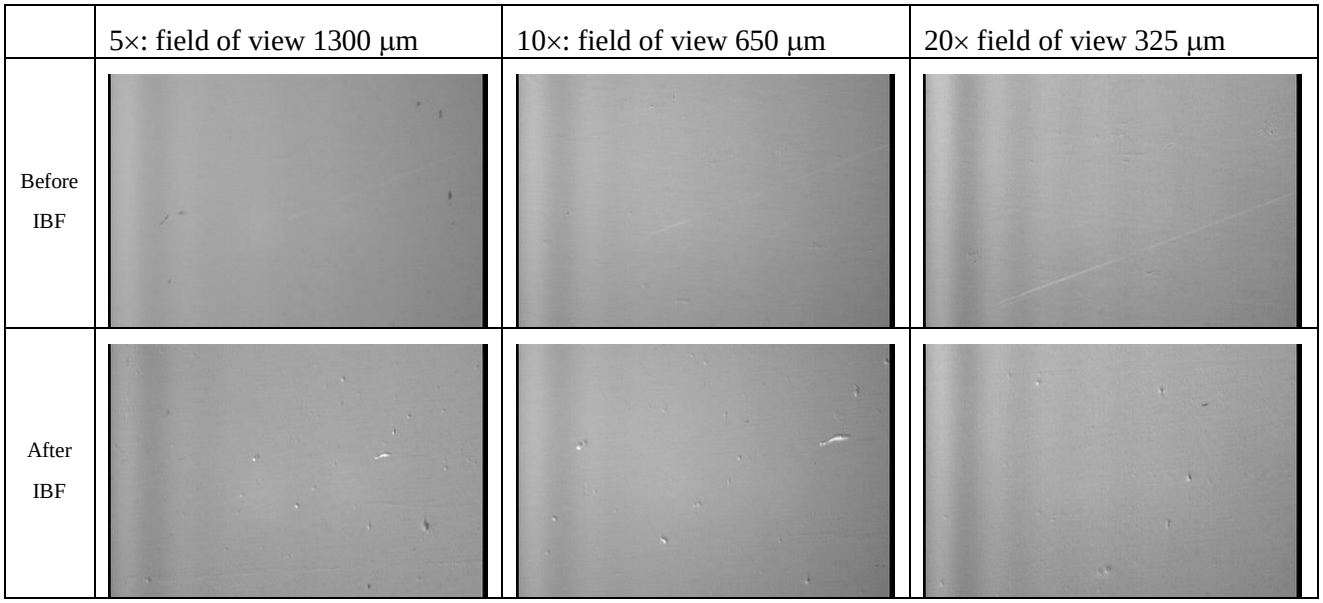

Fig. 2: Nomarsky images of the segment of Fig. 1 before IBF (first row) and after IBF (second row) at different magnifications.

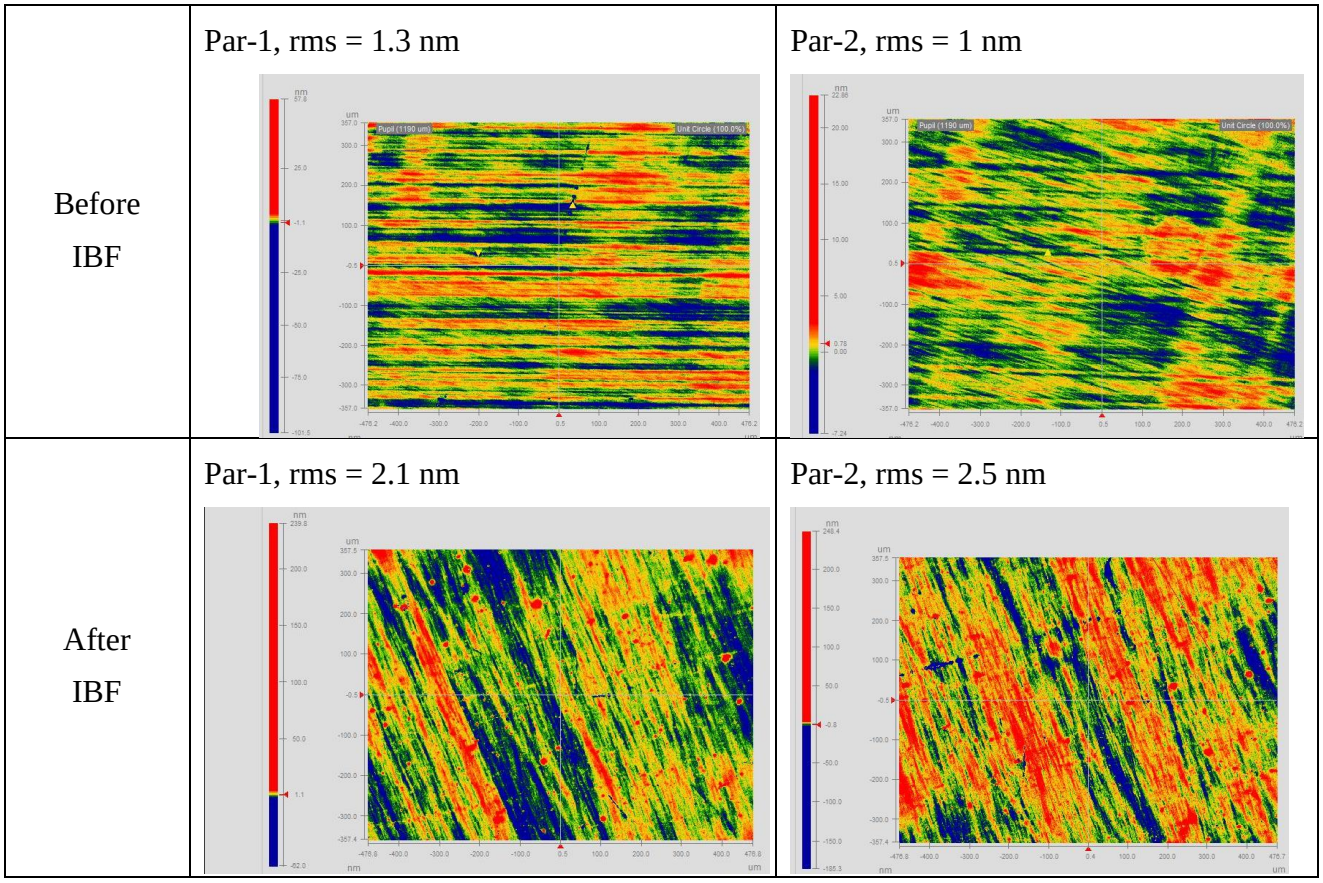

Fig. 3: MFT 10× (field of view 0.71 mm × 0.95 mm) measurements on the parabola side of the segment in Fig. 1, before and after IBF. The original roughness of this segment was about 1.2 nm before IBF, but degraded to 2.3 nm after IBF.

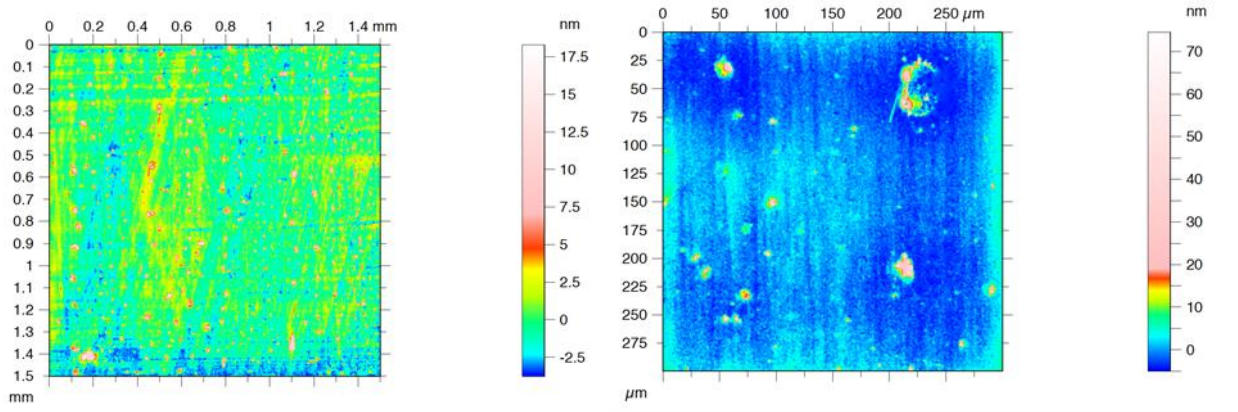

Fig. 4: CCI measurements on the parabola side of the segment in Fig. 1 after IBF. Left: CCI 10× rms = 2.02 nm. Right: CCI 50× rms = 3.71 nm. The original roughness of this segment was near 1.1 nm, as measured with the CCI 50× in a region free from visible defects, confirming the measured rms with the MFT in Fig. 2.

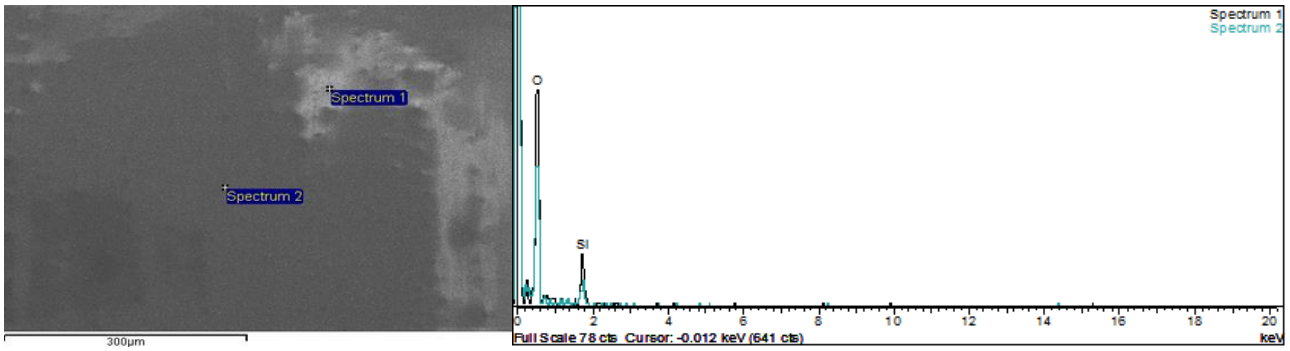

Fig. 5: one of the SEM micro-analyses performed on the segment of Fig. 1 after IBF.

To ascertain the nature of the defects, a SEM micro-analysis was performed at ICMATE (CNR-Lecco). Only Si and O are detected at all positions, ruling out the possibility of chemical contamination of the surface to explain the surface defects visible in the CCI pictures.

3 Roughening of fused silica and other glasses after IBF/RIE: literature search

Several papers were analyzed to reports defects observed on fused silica and other glasses after IBF or Reactive Ion Etching (RIE). [RD2] reports some defects of a few µm wide on fused silica material after IBF/RIE (Fig. 6).

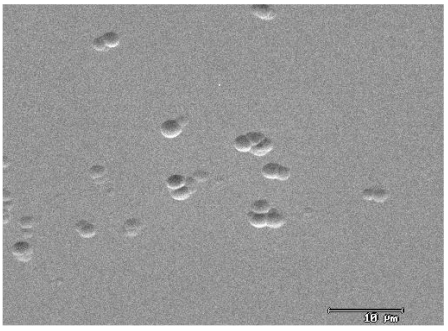

Fig. 6: isolated defects on fused silica after RIE: the removed thickness was 12 µm [RD2].

These defects were observed only when the removed thickness exceeded 3 μm and high beam power was used. The lateral size of the defects was much smaller than in our case (few microns, compared to tens of microns observed in our fused silica segment after IBF). The defects differ also in the shape of the defects: in [RD2] they were pits, whilst in our case they mostly were bulges.

In another paper [RD3], it was shown that defects very similar to Fig. 6 were present after removing few microns with IBF, with pit density dependent to some extent upon the surface preparation technique. It was observed that a surface showing very few defects after polishing could show many surface defects after IBF, with pits apparently following a subsurface scratch or defect in the material. Removing 20-40 μm of material before polishing, however, improves the result of the IBF. RIE is also very much adopted in microelectronics, and glass substrates have to be etched for instance in the contact layer masking process, where boro-phospho-silicate glass (BPSG) is deposited on the wafers, or in Micro Electro-Mechanical Systems (MEMS) devices.

One paper [RD4] shows RIE as performed on a variety of glasses (HOQ310, Suprasil, AF45, D263 and BK7): Fused Silica and Quartz exhibit surface cone-like defects (Fig. 7), with density increasing with decreasing silica quality, while AF45 and BK7 did not. To decrease the defects, a cleaning bath of ammonium fluoride was used to remove the inclusion of abrasive particles left from polishing.

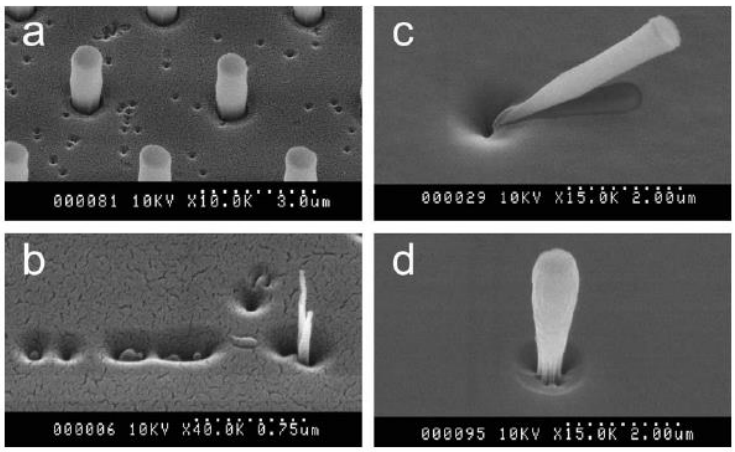

Fig. 7: conical defects formation after RIE is observed on some glass samples, depending on surface preparation [RD4].

In another work [RD5], quartz and Pyrex substrates, masked for microelectronics applications, were processed with RIE using CF_4/Ar and CF_4/O_2 gas mixture. The work shows that the roughening of the masked surface is higher in the case of using Ar with respect to O_2. The effect is ascribed to the larger kinetic energy of the Ar ions, able to produce craters or etching just below the masked area.

Finally, we report a paper showing the roughness evolution after IBF on fused silica optics with small curvature radius [RD6]. The high-slope convex spherical surfaces were figured with two IBF methods, namely three-axis IBF (TIF) and five-axis IBF (FIF). One of the differences between these two methods is the direction of the incidence ion beam: in the TIF, the beam is parallel to the optical axis, while in the FIF it is perpendicular to the local optical surface. Therefore it was possible to investigate the influence of the incidence angle of the ion beam on the surface roughness

of high-slope components during TIF. In Fig. 8, it is visible that at normal and near-normal incidence angles, the surface was smooth on a 2 μm × 2 μm measured area. However, at higher incidence angles, ripples were created with a characteristic period of 33 nm. This pattern was perpendicular to the ion beam direction (indicated by the blue arrow on the Fig. 8a).

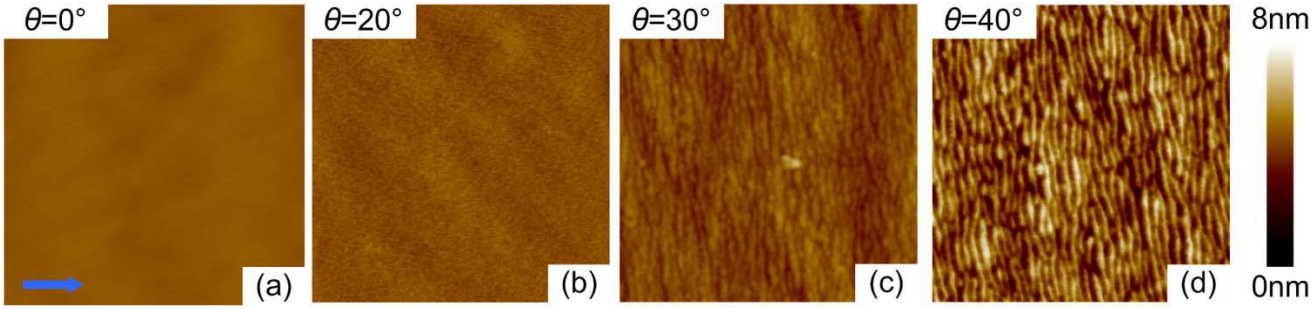

Fig. 8: AFM images of fused silica after TIF at different ion incidence angles; measured area in each case was 2 μm × 2 μm [RD6].

Actually, the Wolter I fused silica segment, figured in OAB with IBF, did not require large incidence angles, and a different defects pattern was observed (Fig. 2-3-4). The literature search here presented suggested that two possible mechanisms could contribute to the observed defects formation:

1) unremoved Sub Surface Damage (SSD), due to the grinding process, producing defects after IBF not visible after the polishing.
2) presence of residuals from the slurry used for the polishing.

In addition, we considered the possibility that some fused silica removed by the IBF could be re-deposited on the sample surfaces.

4 IBF on fused silica flat wafers

Despite the reason that produced the observed defects was not completely clear, we performed tests with the IBF to mitigate the problem. Two flat fused silica wafers were treated with IBF at different distances from the source.

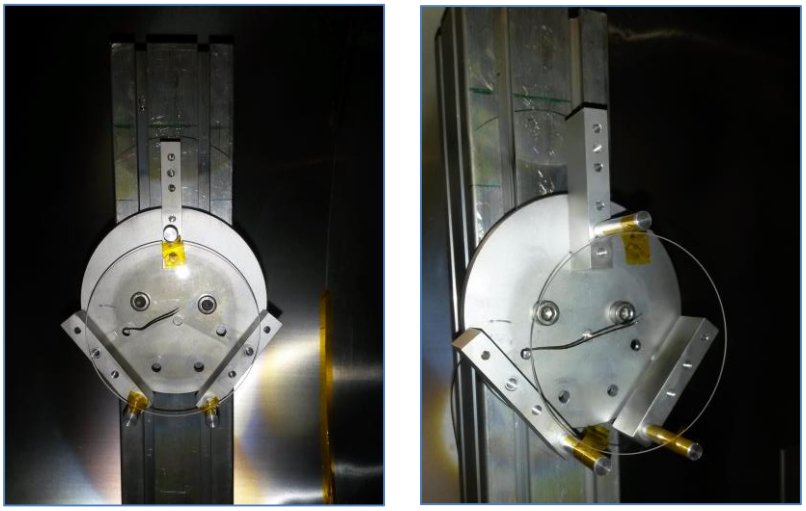

Fig. 9: mounting setup of the flat fused silica wafers on the IBF.

The wafer No. 1 was figured using the 15 mm grids, set at a distance of 36 mm. The power of the beam was 12 W and the electrical setup was the n. 9, i.e.: a beam current of 10 mA, a beam voltage of 1200 V and an accelerating voltage of 100 V. In this test, a constant thickness of 200 nm was removed during 1 h figuring time. This test was done to introduce a thermal stress to the wafer and assess its deformation. After this test, the same sample (No. 1) was used for a second ion beam test with the same parameters, increasing the figuring time to about 5 h, removing about 1 µm of uniform thickness on the sample. The maximum temperature reached on the sample was 140 °C.

The wafer No. 3 was figured at a larger distance (70 mm), again using the setup n. 9. This test was done to evaluate the influence of the distance source-sample on the growth of peaks of fused silica on the sample surface. Again, the figuring time was of about 5 hours and the maximum temperature was of 120 °C. At a distance of 70 mm, the removal rate was smaller, removing a uniform thickness of 660 nm.

5 Roughness characterization of the fused silica flat wafers after IBF

Roughness measurements of the wafers No. 1 and 3 were performed with the MicroFinish Topographer (MFT), with the Mirau 10× magnification objective, thereby obtaining the measured area of about 0.71 mm × 0.95 mm. The results were compared with the rear surface of the wafer No. 2 which was not figured by IBF, and therefore considered as reference. In each case, three spots were measured. The Power Spectral Density (PSD) for each glass was calculated subsequently.

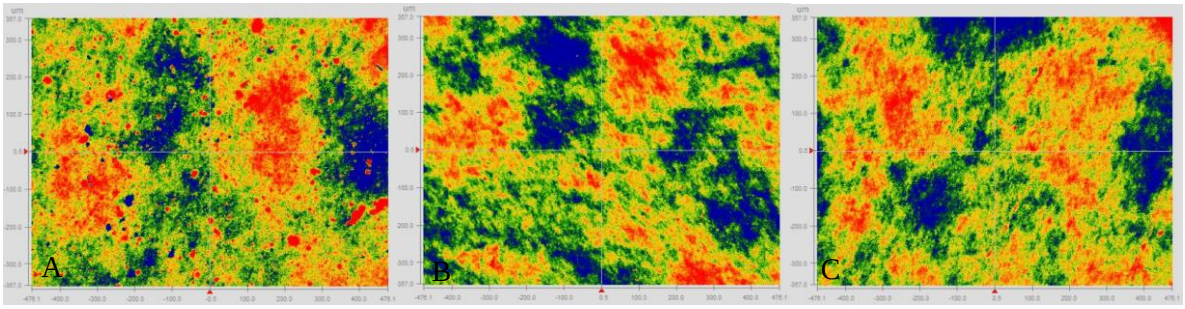

Fig. 10: images of surface obtained with MFT 10×: A) wafer No. 1, B) wafer No. 3, C) wafer No. 2; measured area in each case was 0.71 mm × 0.95 mm.

Table 1. RMS values for each wafer measured with MFT 10×.

	Source – sample distance [mm]	**Max temperature [°C]**	**RMS [nm]**
wafer No. 1	36	140	2.89
wafer No. 3	70	120	1.17
wafer No. 2	no ion beam figuring	no ion beam figuring	0.98

Fig. 10 compares one of the maps obtained on the three Fused Silica flat samples. On the surface of the wafer No. 1 (Fig. 10A) many spots of the size between few and tens of microns are spread over the entire measured area. In the case of the wafer figured at larger distance from the source, the spots are not visible (Fig. 10B), but the rms is slightly higher than the rms of the surface not processed with the ion beam figuring (Fig. 10C). The average rms values, obtained by averaging the PSDs of the measurements on each fused silica plates, are presented in Table 1.

Fig. 11 presents the PSDs of the fused silica wafers in the spatial wavelength range from about 2 μm to 1000 μm. They are compared with the PSD of the WFXT fused silica segment, described in Section 2, after IBF.

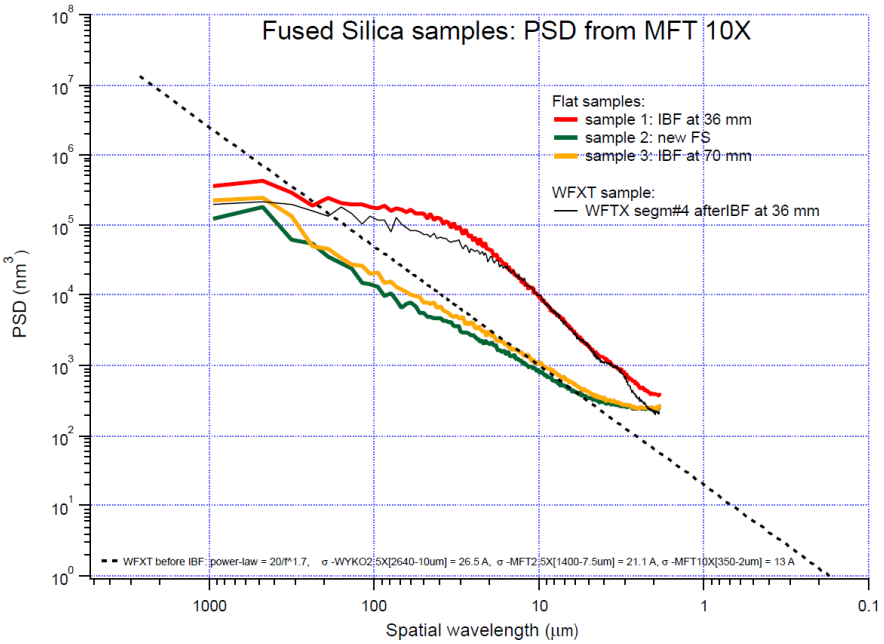

Fig. 11: PSDs of flat fused silica wafers, processed with IBF (red and orange line), compared to the Wolter I WFXT fused silica segment after IBF (black solid line). The unprocessed flat fused silica wafer is shown for comparison (green line), as well as the power law that best fits the roughness data of the WFXT shell before IBF (dashed black line).

As can be observed in Fig. 11, the shape of the PSD for wafer No. 3 is close to the one of the unprocessed wafer. On both surfaces neither bumps nor pits were noticed. The amplitude of the surface roughness of wafer No. 1 is instead higher in the measured spatial wavelengths range. Moreover, the PSD of the WFXT segment after IBF well matches the PSD of sample No. 1. Both WFXT and sample No. 1 have a similar surface topography that could be observed in the MFT images.

From Fig. 11 it can be easily seen that increasing the distance between the workpiece and the ion beam source has effectively reduced the amplitude of the roughness almost to the level of the untouched glass. Increasing the sample-source distance from 36 mm to 70 mm, there is also a reduction in the maximum temperature reached on the glass sample during the IBF process. The maximum temperature decreased from 140 °C to 120 °C, which also could have an impact on the defect generation.

6 Conclusions

A severe roughness degradation was observed after IBF on a Wolter I Fused Silica segment, figured at 36 mm distance from the ion source. In order to investigate the reason, a literature search was carried out that suggested three possible mechanisms: 1) unremoved SSD, 2) presence of residuals from the slurry used for the polishing, 3) re-deposition of Fused Silica removed by the IBF. To mitigate the problem, two flat fused silica wafers were processed with IBF at two different

distances from the ion source. Three areas, in size of almost 1 mm^2, were measured with the MFT (10× objective) on all the samples. The average PSD was calculated for each glass. A degradation of the surface roughness, similar for the flat and the Wolter I samples, was observed when figuring at 36 mm distance. In the images taken by MFT, bumps in size from few to tens microns were visible on both flat and curved samples.

In order to improve the surface quality, the sample-source distance was increased from 36 mm to 70 mm. The PSD of the fused silica wafer figured at 70 mm was very close to the one measured on a brand-new fused silica wafer, showing that the degradation can be almost completely avoided increasing the sample-source distance.